Frictional Contact-Implicit Inverse Dynamics via Complementarity-Constrained Optimization

Pierre Fabre[1], Etienne Ménager[1], Antoine Bambade[2], Wilson Jallet[1], Alberto De Marchi[3] and Justin Carpentier[1]

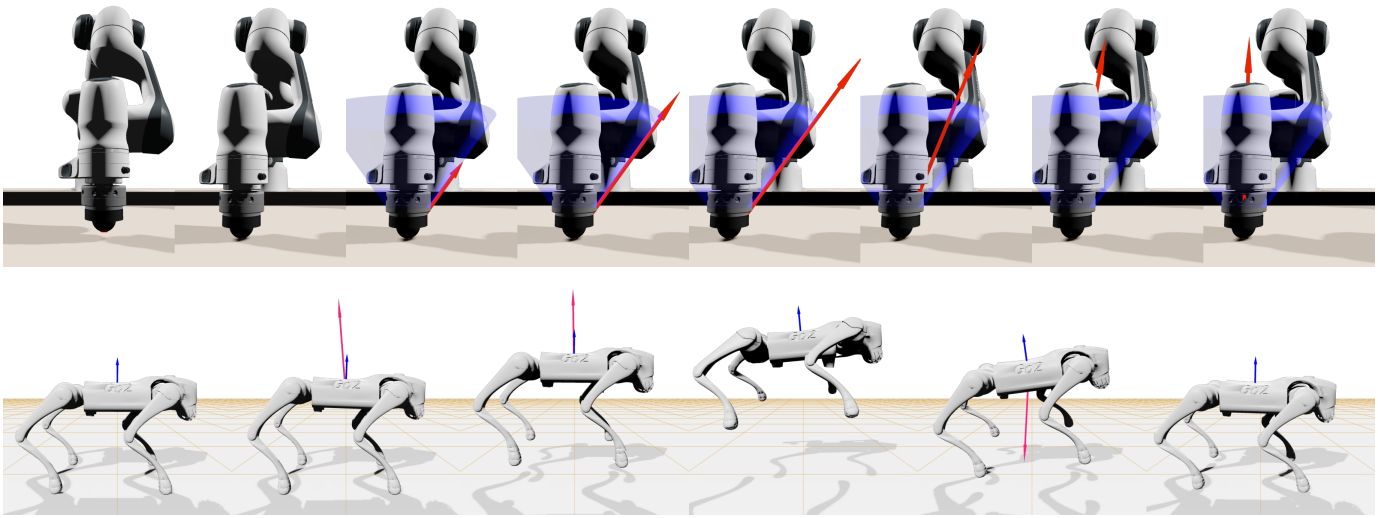

Fig. 1: **Franka sanding task (Top).** The robot first makes contact with the ground, then starts sliding towards the left, which makes the reaction force lie on the boundary of the friction cone $\partial\mathcal{K}_\mu$. Then the robot comes to rest on the surface, the contact force vector lies strictly within the friction cone and transitions smoothly to its center. **Go2 jumping task (Bottom).** Time-lapse of the contact-implicit inverse dynamics controller running in simulation, tracking a desired altitude for the base. The controller automatically determines that contacts must be broken and initiates a jump.

***Abstract*—Task-space inverse dynamics is a versatile paradigm for real-time robot control, capable of handling underactuation and contact interactions in complex environments. However, existing contact-aware controllers typically rely on predefined contact sequences or simplified contact models, limiting their ability to capture rich frictional behaviors. In this work, we formulate frictional contact-implicit inverse dynamics as a quadratic program with complementarity constraints (QPCC), modeling unilateral contact and Coulomb friction through a nonlinear complementarity constraint. This novel approach avoids the simplifying assumptions commonly used in prior work, enabling richer modeling of frictional behavior.**

To solve the resulting nonsmooth and nonconvex problem, we propose an approach based on the augmented Lagrangian method (ALM) combined with alternating minimization. Our solver alternates between minimizing a smooth, convex function that captures task objectives and system dynamics, and projecting onto sets that enforce actuation and frictional contact constraints. By handling complementarity constraints through projection, the method implicitly and automatically reasons over contact modes (sticking, sliding, and breaking).

We demonstrate the efficiency and versatility of the proposed approach across a range of contact-rich robotic scenarios. This work highlights the potential of complementarity-constrained optimization as a practical framework for contact-implicit control.

***Index Terms*—Numerical optimization, Robot control, Contact dynamics**

[1]Inria and Département d'Informatique de l'École Normale Supérieure, PSL Research University in Paris, 75013 Paris, France.

[2]work done while at EDF Lab, 7 boulevard Gaspard Monge, 91120 Palaiseau, France.

[3]University of the Bundeswehr Munich, Department of Aerospace Engineering, Institute of Applied Mathematics and Scientific Computing, 85577 Neubiberg, Germany.

I. Background and Related Work

Contact modeling is central to the simulation and control of robotic systems that interact with their environment through intermittent and frictional contacts. Accurately capturing these interactions is essential for realistic simulation and robust control in applications such as manipulation and locomotion [1]. However, frictional contact leads to inherently nonlinear, nonsmooth, and nonconvex dynamics, making control in contact-rich environments particularly challenging.

Contact dynamics are commonly formulated as complementarity problems, either as linear (LCP) or nonlinear (NCP), where contact forces and velocities are coupled through the system dynamics. In this work, we show that task-space inverse dynamics with frictional contact can be naturally formu-

lated as a quadratic program with complementarity constraints (QPCC), a particular instance of mathematical programs with complementarity constraints (MPCC). This formulation captures unilateral contact and Coulomb friction through cone complementarity constraints, enabling a physically consistent description of sticking, sliding, and breaking modes.

From an optimization perspective, MPCCs are challenging due to the nonconvexity of their feasible set and the failure of standard constraint qualifications [2]. Existing approaches typically rely on relaxations or smoothing strategies, such as penalty or homotopy methods [3]–[6], or mixed-integer formulations that do not scale well.

In robotics, prior work has studied inverse dynamics under contact mainly in joint space using impulse-based formulations [7], [8]. In contrast, task-space inverse dynamics (operational-space control) enables direct tracking of task objectives but typically assumes predefined contact sequences [9]–[11]. Contact-implicit formulations remove this assumption and allow automatic reasoning over contact modes, but existing methods often rely on simplified or smooth approximations of contact dynamics [12]–[15], which may compromise physical fidelity.

Our approach instead adheres to a nonsmooth complementarity formulation of frictional contact and casts the problem as a QPCC. To solve it, we draw inspiration from augmented Lagrangian methods and splitting techniques, which have proven effective for structured optimization problems. In particular, our method alternates between solving a quadratic program (QP) capturing system dynamics and task objectives, and projecting onto sets enforcing actuator limits and complementarity constraints. This enables implicit and physically consistent reasoning over contact modes without relying on smoothing or relaxation.

This paper is based on a larger work that has been submitted to *IEEE Transactions on Robotics* (T-RO) and is currently under review. For more detailed derivations and experiments, please refer to the preprint [16].

II. Dynamics and Contact Modeling

Rigid-body dynamics. We consider a multi-body robotic system with configuration $\boldsymbol{q}$ and generalized velocity $\boldsymbol{v}$. The positions of contact points are denoted $\boldsymbol{c}(\boldsymbol{q}) \in \mathbb{R}^{3n_c}$, with associated Jacobian $J_c = \partial \boldsymbol{c}/\partial \boldsymbol{q}$. The Lagrangian dynamics are given by

$$M(\boldsymbol{q})\dot{\boldsymbol{v}} + \boldsymbol{b}(\boldsymbol{q}, \boldsymbol{v}) = J_a^\top(\boldsymbol{q})\boldsymbol{\tau} + J_c^\top(\boldsymbol{q})\boldsymbol{f}_c, \tag{1}$$

where M is the inertia matrix, $\boldsymbol{b}$ gathers Coriolis and gravity terms, $\boldsymbol{\tau}$ are joint torques mapped by the actuation matrix J_a, and $\boldsymbol{f}_c$ are contact forces. For readability, dependencies in $(\boldsymbol{q}, \boldsymbol{v})$ are omitted in the following.

Using a semi-implicit Euler discretization with time step Δt, the dynamics can be written as

$$\boldsymbol{v}^+ = \boldsymbol{v} + M^{-1}(J_a^\top \boldsymbol{\tau} + J_c^\top \boldsymbol{f}_c - \boldsymbol{b})\Delta t. \tag{2}$$

Impulse formulation. Following [8], introducing the free velocity $\boldsymbol{v}_{fr} = \boldsymbol{v} - M^{-1}\boldsymbol{b}\Delta t$, impulse torques $\boldsymbol{\lambda}_a = \boldsymbol{\tau}\Delta t$ and impulse contact forces $\boldsymbol{\lambda}_c = \boldsymbol{f}_c\Delta t$, the dynamics become

$$\boldsymbol{v}^+ = \boldsymbol{v}_{fr} + M^{-1}(J_a^\top \boldsymbol{\lambda}_a + J_c^\top \boldsymbol{\lambda}_c). \tag{3}$$

Frictional contact model. The contact-point velocity is defined as

$$\boldsymbol{\sigma} = J_c\boldsymbol{v}^+ + \boldsymbol{\gamma}_c \quad \text{with} \quad \boldsymbol{\gamma}_c = \begin{bmatrix} \boldsymbol{0} & \frac{c_N}{\Delta t} \end{bmatrix}, \tag{4}$$

where $\begin{bmatrix} \boldsymbol{x}_T & x_N \end{bmatrix}$ is the tangential/normal decomposition of a vector $\boldsymbol{x}$. Substituting (3) in (4) yields

$$\boldsymbol{\sigma} = J_c\boldsymbol{v}_{fr} + J_c M^{-1}(J_a^\top \boldsymbol{\lambda}_a + J_c^\top \boldsymbol{\lambda}_c) + \boldsymbol{\gamma}_c, \tag{5}$$

where $J_c M^{-1} J_c^\top$ is the Delassus matrix [17] that gives the system inertia projected on the contacts, linking contact forces to contact point velocities.

Frictional contact is governed by three principles:

- **Signorini:** $0 \leq \lambda_N \perp \sigma_N \geq 0$, ensures the normal force is repulsive, bodies do not interpenetrate, and no simultaneous separation motion and contact force exist. Signorini condition alone can be handled as an LCP. Expressed in velocity thanks to the definition of (4),
- **Coulomb friction:** $\|\boldsymbol{\lambda}_T\|_2 \leq \mu\lambda_N$, characterized by the so-called friction coefficient μ, states that the tangential force component is bounded by the normal force value Contact forces lie inside a second-order cone,
- **Maximum dissipation:** $\boldsymbol{\lambda}_T \in \operatorname{argmax}_{\|\boldsymbol{y}\|_2 \leq \mu\lambda_N} -\boldsymbol{y}^T\boldsymbol{\sigma}_T$ states that the tangential force maximizes the power dissipated by the contact.

These conditions can be compactly expressed as a nonlinear complementarity problem (NCP):

$$\mathcal{K}_\mu \ni \boldsymbol{\lambda} \perp \boldsymbol{\sigma} + \Gamma_\mu(\boldsymbol{\sigma}) \in \mathcal{K}_\mu^*, \tag{6}$$

where $\mathcal{K}_\mu$ is the Coulomb friction cone, $\mathcal{K}_\mu^* = \mathcal{K}_{\frac{1}{\mu}}$ its dual cone, and $\Gamma_\mu(\boldsymbol{\sigma}) = \begin{bmatrix} \boldsymbol{0} & \mu\|\boldsymbol{\sigma}_T\|_2 \end{bmatrix}$ is the De Saxcé correction [18]. The NCP can be relaxed into a conic complementarity problem (CCP) by removing the De Saxcé correction or into a LCP by using a polyhedral approximation of the Coulomb cone. Both lead to non-physical effects [1].

Contact modes. The complementarity conditions induce three mutually exclusive regimes illustrated in Fig. 2.

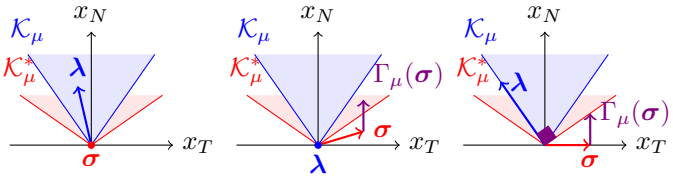

Sticking $\boldsymbol{\lambda} \in \mathcal{K}_\mu$, $\boldsymbol{\sigma} + \Gamma_\mu(\boldsymbol{\sigma}) = \boldsymbol{0}$

Breaking $\boldsymbol{\lambda} = \boldsymbol{0}$, $\boldsymbol{\sigma} + \Gamma_\mu(\boldsymbol{\sigma}) \in \mathcal{K}_\mu^*$

Sliding $\boldsymbol{\lambda} \in \partial\mathcal{K}_\mu$, $\boldsymbol{\sigma} + \Gamma_\mu(\boldsymbol{\sigma}) \in \partial\mathcal{K}_\mu^*$

Fig. 2: The three contact modes illustrated using the NCP formulation. Contact forces $\boldsymbol{\lambda}$ (blue) and velocities $\boldsymbol{\sigma}$ (red) are constrained by the friction cone $\mathcal{K}_\mu$ and its dual $\mathcal{K}_\mu^*$, with the De Saxcé correction Γ_μ shown in purple.

III. Contact-Implicit Inverse Dynamics

Problem statement. Let $p_{ee}(\boldsymbol{q})$ be the positions or poses (e.g., a Cartesian product of $\mathbb{R}^3$ or $\mathrm{SE}(3)$) of the end-effectors in configuration $\boldsymbol{q}$, and J_{ee} the Jacobian of p_{ee}. Using the impulse-based dynamics introduced previously, we formulate task-space inverse dynamics with frictional contact as the following QPCC:

$$\begin{aligned} \underset{\boldsymbol{v}^+,\boldsymbol{\lambda}_a,\boldsymbol{\lambda}_c}{\text{minimize}} \quad & \frac{1}{2}\|J_{ee}\boldsymbol{v}^+ + \boldsymbol{b}_{ee}\|_{W_v}^2 \\ \text{subject to} \quad & \boldsymbol{v}^+ = M^{-1}J_a^\top \boldsymbol{\lambda}_a + M^{-1}J_c^\top \boldsymbol{\lambda}_c + \boldsymbol{v}_{fr}, \\ & \boldsymbol{\sigma} = J_c\boldsymbol{v}^+ + \boldsymbol{\gamma}_c, \\ & \mathcal{K}_\mu \ni \boldsymbol{\lambda}_c \perp \boldsymbol{\sigma} + \Gamma_\mu(\boldsymbol{\sigma}) \in \mathcal{K}_\mu^*, \\ & \boldsymbol{\lambda}_a \in \mathbb{B}, \end{aligned} \tag{7}$$

with motor torque impulses limits $\mathbb{B} \triangleq [\boldsymbol{\tau}_{\min}\Delta t, \boldsymbol{\tau}_{\max}\Delta t]$ and drift term $\boldsymbol{b}_{ee}$. We also add optional regularization/tracking terms $\frac{1}{2}\|\boldsymbol{\lambda} - \bar{\boldsymbol{\lambda}}\|_W^2$ for both torques $\boldsymbol{\lambda}_a$ and contact forces $\boldsymbol{\lambda}_c$. Substituting (3) in (7) yields the reduced QPCC[1]:

$$\begin{aligned} \underset{\boldsymbol{\lambda}_a,\boldsymbol{\lambda}_c}{\text{minimize}} \quad & \frac{1}{2}\|A\boldsymbol{\lambda}_a + B\boldsymbol{\lambda}_c + \boldsymbol{b}\|_2^2 \\ \text{subject to} \quad & \boldsymbol{\sigma} = C\boldsymbol{\lambda}_a + D\boldsymbol{\lambda}_c + \boldsymbol{g}, \\ & \mathcal{K}_\mu \ni \boldsymbol{\lambda}_c \perp \boldsymbol{\sigma} + \Gamma_\mu(\boldsymbol{\sigma}) \in \mathcal{K}_\mu^*, \\ & \boldsymbol{\lambda}_a \in \mathbb{B}. \end{aligned} \tag{8}$$

Splitting. To handle the complementarity constraints, we introduce a slack variable $\boldsymbol{\sigma}$ and the following variable splitting:

$$\begin{aligned} \underset{\substack{\boldsymbol{\lambda}_a,\boldsymbol{\lambda}_c,\boldsymbol{\sigma} \\ \hat{\boldsymbol{\lambda}}_a,\hat{\boldsymbol{\lambda}}_c,\hat{\boldsymbol{\sigma}}}}{\text{minimize}} \quad & F(\boldsymbol{\lambda}_a,\boldsymbol{\lambda}_c,\boldsymbol{\sigma}) + \mathcal{I}_{\mathbb{S}}(\hat{\boldsymbol{\lambda}}_a,\hat{\boldsymbol{\lambda}}_c,\hat{\boldsymbol{\sigma}}) \\ \text{subject to} \quad & \boldsymbol{\lambda}_a = \hat{\boldsymbol{\lambda}}_a,\ \boldsymbol{\lambda}_c = \hat{\boldsymbol{\lambda}}_c,\ \boldsymbol{\sigma} = \hat{\boldsymbol{\sigma}}, \end{aligned} \tag{9}$$

where $\mathcal{I}$ is the indicator function, $\mathbb{S}_c$ is the nonlinear complementarity set, $\mathbb{S} \triangleq \mathbb{S}_c \times \mathbb{B}$ and $F(\boldsymbol{\lambda}_a,\boldsymbol{\lambda}_c,\boldsymbol{\sigma}) \triangleq \frac{1}{2}\|A\boldsymbol{\lambda}_a + B\boldsymbol{\lambda}_c + \boldsymbol{b}\|_2^2 + \mathcal{I}_{\{\boldsymbol{\sigma}=C\boldsymbol{\lambda}_a+D\boldsymbol{\lambda}_c+\boldsymbol{g}\}}$. The auxiliary variables $\hat{\boldsymbol{\lambda}}_a, \hat{\boldsymbol{\lambda}}_c, \hat{\boldsymbol{\sigma}}$ serve to decouple the smooth dynamics from the nonsmooth complementarity constraints.

Augmented Lagrangian. To tackle the optimization problem (9) we use the associated Augmented Lagrangian $\mathcal{L}_{\xi,\eta,\rho}$ (see Ch. 17.3 in [19]) defined as:

$$\begin{aligned} &\mathcal{L}_{\xi,\eta,\rho}(\boldsymbol{\lambda}_a,\boldsymbol{\lambda}_c,\boldsymbol{\sigma},\hat{\boldsymbol{\lambda}}_a,\hat{\boldsymbol{\lambda}}_c,\hat{\boldsymbol{\sigma}},\boldsymbol{y}_a,\boldsymbol{y}_c,\boldsymbol{y}_\sigma) \\ &\quad \triangleq F(\boldsymbol{\lambda}_a,\boldsymbol{\lambda}_c,\boldsymbol{\sigma}) + \mathcal{I}_{\mathbb{S}}(\hat{\boldsymbol{\lambda}}_a,\hat{\boldsymbol{\lambda}}_c,\hat{\boldsymbol{\sigma}}) \\ &\quad + \boldsymbol{y}_a^\top(\boldsymbol{\lambda}_a - \hat{\boldsymbol{\lambda}}_a) + \boldsymbol{y}_c^\top(\boldsymbol{\lambda}_c - \hat{\boldsymbol{\lambda}}_c) + \boldsymbol{y}_\sigma^\top(\boldsymbol{\sigma} - \hat{\boldsymbol{\sigma}}) \\ &\quad + \frac{\xi}{2}\|\boldsymbol{\lambda}_a - \hat{\boldsymbol{\lambda}}_a\|^2 + \frac{\eta}{2}\|\boldsymbol{\lambda}_c - \hat{\boldsymbol{\lambda}}_c\|^2 + \frac{\rho}{2}\|\boldsymbol{\sigma} - \hat{\boldsymbol{\sigma}}\|^2, \end{aligned} \tag{10}$$

[1]In [16], we show that our formulations also apply in soft robotics.

where $\boldsymbol{y}_a, \boldsymbol{y}_c, \boldsymbol{y}_\sigma$ and ξ, η, ρ are respectively the multipliers and penalty parameters associated with the splitting.

Alternating minimization. The inner loop of our algorithm alternates between two steps:

Step 1: Smooth QP. Solve a quadratic program enforcing dynamics and task objectives

$$\begin{aligned} \underset{\boldsymbol{\lambda}_a,\boldsymbol{\lambda}_c,\boldsymbol{\sigma}}{\text{argmin}} \quad & \frac{1}{2}\|A\boldsymbol{\lambda}_a + B\boldsymbol{\lambda}_c + \boldsymbol{b}\|_2^2 + \frac{\xi_k}{2}\left\|\boldsymbol{\lambda}_a - \hat{\boldsymbol{\lambda}}_a^k + \frac{\boldsymbol{y}_a^k}{\xi_k}\right\|_2^2 \\ & + \frac{\eta_k}{2}\left\|\boldsymbol{\lambda}_c - \hat{\boldsymbol{\lambda}}_c^k + \frac{\boldsymbol{y}_c^k}{\eta_k}\right\|_2^2 + \frac{\rho_k}{2}\left\|\boldsymbol{\sigma} - \hat{\boldsymbol{\sigma}}^k + \frac{\boldsymbol{y}_\sigma^k}{\rho_k}\right\|_2^2 \\ \text{s.t.} \quad & \boldsymbol{\sigma} = C\boldsymbol{\lambda}_a + D\boldsymbol{\lambda}_c + \boldsymbol{g}. \end{aligned} \tag{11}$$

This step reduces to solving a structured linear system with a symmetric quasi-definite matrix.

Step 2: Projection. Project onto the constraint set $\mathbb{S} = \mathbb{B} \times \mathbb{S}_c$. This is equivalent to two separate projections: first onto the actuator bounds $\mathbb{B}$ and then onto the frictional contact set $\mathbb{S}_c$:

$$\begin{aligned} &\underset{\hat{\boldsymbol{\lambda}}_a \in \mathbb{B}}{\text{argmin}} \ \frac{\xi_k}{2}\left\|\boldsymbol{\lambda}_a^k + \frac{\boldsymbol{y}_a^k}{\xi_k} - \hat{\boldsymbol{\lambda}}_a\right\|_2^2, \\ &\underset{(\hat{\boldsymbol{\lambda}}_c,\hat{\boldsymbol{\sigma}}) \in \mathbb{S}_c}{\text{argmin}} \underbrace{\frac{\eta_k}{2}\left\|\boldsymbol{\lambda}_c^k + \frac{\boldsymbol{y}_c^k}{\eta_k} - \hat{\boldsymbol{\lambda}}_c\right\|_2^2 + \frac{\rho_k}{2}\left\|\boldsymbol{\sigma}^k + \frac{\boldsymbol{y}_\sigma^k}{\rho_k} - \hat{\boldsymbol{\sigma}}\right\|_2^2}_{\triangleq \mathcal{P}(\hat{\boldsymbol{\lambda}}_c,\hat{\boldsymbol{\sigma}})}. \end{aligned} \tag{12}$$

The projection onto $\mathbb{S}_c$ is challenging due to its nonsmooth and nonconvex nature. To illustrate this, we consider the simpler frictionless (Signorini-only) case, which reduces to a LCP. The projection onto this set, shown in Fig. 3, will serve as a guide for the NCP case.

Contact projection via mode enumeration. Since no closed-form projection exists, we compute it by evaluating the value of $\mathcal{P}(\hat{\boldsymbol{\lambda}}_c, \hat{\boldsymbol{\sigma}})$ for each contact mode:

- **Sticking:** $\mathcal{P}\left(\mathrm{proj}_{\mathcal{K}_\mu}\left(\boldsymbol{\lambda}_c^k + \frac{\boldsymbol{y}_c^k}{\eta_k}\right), \boldsymbol{0}\right)$,
- **Breaking:** $\mathcal{P}\left(\boldsymbol{0}, \mathrm{proj}_{\mathbb{R}^2 \times \mathbb{R}_+}\left(\boldsymbol{\sigma}^k + \frac{\boldsymbol{y}_\sigma^k}{\rho_k}\right)\right)$,
- **Sliding:** $\min_{\boldsymbol{\sigma}_T, \lambda_N} \mathcal{P}\left(\begin{bmatrix} -\mu\lambda_N \frac{\boldsymbol{\sigma}_T}{\|\boldsymbol{\sigma}_T\|_2} & \lambda_N \end{bmatrix}, \begin{bmatrix} \boldsymbol{\sigma}_T & 0 \end{bmatrix}\right)$.

The optimal projection is obtained by selecting the minimizer. This procedure is performed independently at each contact point and can be parallelized.

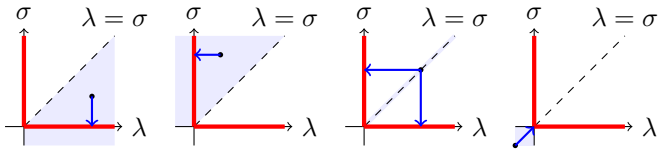

Fig. 3: Orthogonal projection of (λ, σ) (black dot) onto the nonconvex feasible set (red) defined by the LCP (Signorini-only). Blue arrows indicate the projections, and shaded regions illustrate the partition of the space.

Algorithm. The method follows a two-level scheme. An inner loop alternates between the quadratic minimization step and the projection onto the constraint set until a given tolerance is met. An outer loop updates the multipliers, penalty parameters and tolerances using a Bound-Constrained Lagrangian (BCL) strategy [20].

IV. Experiments

We evaluate the proposed contact-implicit inverse dynamics solver on several robotics contact-rich tasks, highlighting its versatility. The solver is implemented in C++ using Eigen [21] and integrated with Pinocchio [22] for rigid-body dynamics and Coal [23] for collision detection. All experiments are run in closed loop with an integration time step $\Delta t = 10^{-3}$ seconds inside the Simple simulator [8].

Franka sanding. We consider a 6D tracking task where the end-effector makes contact with a surface and slides while tracking a normal force. The proposed method successfully captures sliding contact and produces consistent force tracking, illustrating the benefits of the NCP formulation (see Fig. 1 and Fig. 4). We also validate the approach on hardware, showing good agreement with simulation in terms of motion and contact behavior.

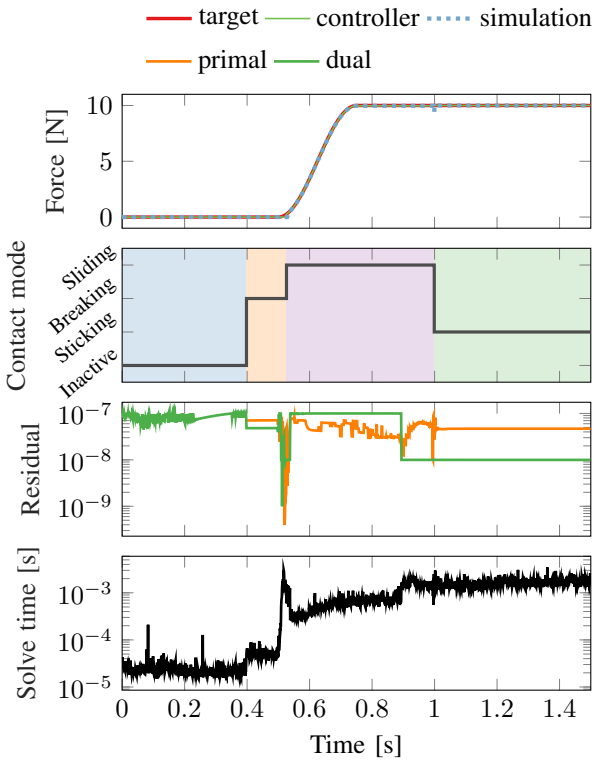

Fig. 4: **Franka sanding task (simulation). Top row.** z-direction ground reaction force (target, controller output, simulation value). **Second row.** Controller's inferred contact mode. **Third row.** Primal and dual feasibility measures. **Bottom row.** ALM solver wall times.

Go2 jumping. We evaluate the ability of the method to handle contact switching on a quadruped robot. The controller successfully generates dynamic motions and automatically breaks and re-establishes contacts while tracking the desired base motion (see Fig. 1 and Fig. 5).

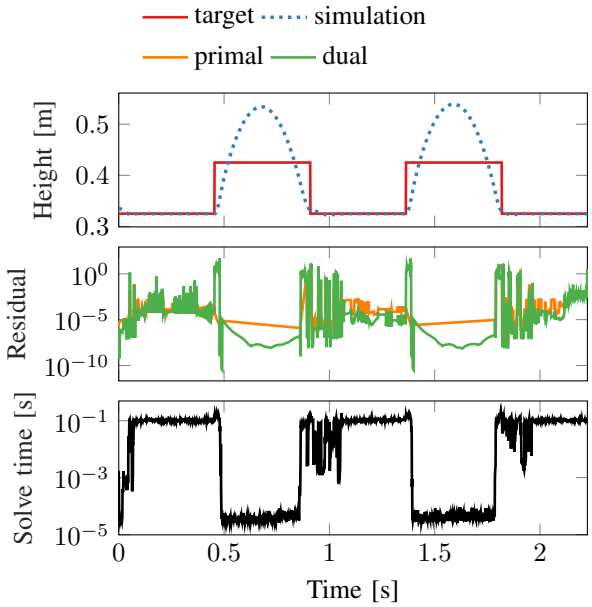

Fig. 5: **Go2 jumping task. Top:** Task target and simulator response. **Middle:** Primal and dual feasibility measures. **Bottom:** ALM solver wall time.

V. Conclusion

We presented a QPCC formulation of contact-implicit task-space inverse dynamics that explicitly handles frictional contact and actuator limits. By directly tackling the NCP, the proposed approach captures physically consistent contact behaviors without resorting to smoothing or relaxation. To solve the resulting nonsmooth and nonconvex problem, we introduced an augmented Lagrangian method combined with alternating minimization. This splitting enables efficient enforcement of complementarity constraints via projection, while implicitly recovering contact modes such as sticking, sliding, and breaking. Experiments on contact-rich robotic scenarios demonstrate that the method produces realistic behaviors while achieving task-space tracking objectives, highlighting its potential for practical contact-implicit control. Future work will focus on extending the approach to trajectory optimization, improving computational performance, and validating the method on more complex real-world robotic tasks.

Acknowledgment

The authors sincerely thank Timothée Carecchio for his essential contribution to the realization of the Franka sanding experiments on hardware. His technical expertise and dedication were key to successfully transferring the task from simulation to the real robot.

REFERENCES

[1] Q. Le Lidec, W. Jallet, L. Montaut, I. Laptev, C. Schmid, and J. Carpentier, "Contact Models in Robotics: A Comparative Analysis," *IEEE Transactions on Robotics*, vol. 40, pp. 3716–3733, Jul. 2024.

[2] J. J. Ye, D. L. Zhu, and Q. J. Zhu, "Exact penalization and necessary optimality conditions for generalized bilevel programming problems," *SIAM Journal on Optimization*, vol. 7, no. 2, pp. 481–507, 1997.

[3] M. Anitescu, "On using the elastic mode in nonlinear programming approaches to mathematical programs with complementarity constraints," *SIAM Journal on Optimization*, vol. 15, no. 4, pp. 1203–1236, 2005.

[4] C. Kanzow and A. Schwartz, "A new regularization method for mathematical programs with complementarity constraints with strong convergence properties," *SIAM Journal on Optimization*, vol. 23, no. 2, pp. 770–798, 2013.

[5] K. Lin and T. Ohtsuka, "A gap penalty method for optimal control of linear complementarity systems," in *2024 IEEE 63rd Conference on Decision and Control (CDC)*, 2024, pp. 880–887.

[6] A. Nurkanović, A. Pozharskiy, and M. Diehl, "Solving Mathematical Programs with Complementarity Constraints Arising in Nonsmooth Optimal Control," *Vietnam Journal of Mathematics*, vol. 53, no. 3, pp. 659–697, Jul. 2025.

[7] E. Todorov, "Convex and analytically-invertible dynamics with contacts and constraints: Theory and implementation in MuJoCo," in *2014 IEEE International Conference on Robotics and Automation (ICRA)*. IEEE, 2014, pp. 6054–6061.

[8] J. Carpentier, L. Montaut, and Q. L. Lidec, "From compliant to rigid contact simulation: a unified and efficient approach," *Robotics: Science and Systems*, 2024.

[9] R. Budhiraja, J. Carpentier, C. Mastalli, and N. Mansard, "Differential dynamic programming for multi-phase rigid contact dynamics," in *2018 IEEE-RAS 18th International Conference on Humanoid Robots (Humanoids)*. IEEE, 2018, pp. 1–9.

[10] J. Carpentier and P.-B. Wieber, "Recent progress in legged robots locomotion control," *Current Robotics Reports*, vol. 2, no. 3, pp. 231–238, 2021.

[11] P. M. Wensing, M. Posa, Y. Hu, A. Escande, N. Mansard, and A. Del Prete, "Optimization-based control for dynamic legged robots," *IEEE Transactions on Robotics*, vol. 40, pp. 43–63, 2023.

[12] E. Todorov, "Goal directed dynamics," in *2018 IEEE International Conference on Robotics and Automation (ICRA)*, 2018, pp. 2994–3000.

[13] S. Le Cleac'h, T. A. Howell, S. Yang, C.-Y. Lee, J. Zhang, A. Bishop, M. Schwager, and Z. Manchester, "Fast contact-implicit model predictive control," *IEEE Transactions on Robotics*, vol. 40, pp. 1617–1629, 2024.

[14] V. Kurtz, A. Castro, A. Ö. Önol, and H. Lin, "Inverse Dynamics Trajectory Optimization for Contact-Implicit Model Predictive Control," May 2025.

[15] A. Aydinoglu, A. Wei, W.-C. Huang, and M. Posa, "Consensus complementarity control for multicontact mpc," *IEEE Transactions on Robotics*, vol. 40, pp. 3879–3896, 2024.

[16] E. Ménager, P. Fabre, A. Bambade, W. Jallet, A. de Marchi, and J. Carpentier, "Frictional Contact-Implicit Inverse Dynamics," Aug. 2025, working paper or preprint. [Online]. Available: https://hal.science/hal-05201780

[17] É. Delassus, "Mémoire sur la théorie des liaisons finies unilatérales," *Ann. Sci. Ec. Norm. Super. (4)*, vol. 34, pp. 95–179, 1917.

[18] G. De Saxcé and Z.-Q. Feng, "The bipotential method: A constructive approach to design the complete contact law with friction and improved numerical algorithms," *Mathematical and Computer Modelling*, vol. 28, no. 4, pp. 225–245, 1998, recent Advances in Contact Mechanics.

[19] J. Nocedal and S. J. Wright, *Numerical Optimization*, second edition ed., ser. Springer Series in Operations Research and Financial Engineering. New York, NY: Springer, 2006.

[20] A. R. Conn, N. I. M. Gould, and P. L. Toint, "A globally convergent augmented Lagrangian algorithm for optimization with general constraints and simple bounds," *SIAM Journal on Numerical Analysis*, vol. 28, no. 2, pp. 545–572, 1991.

[21] G. Guennebaud, B. Jacob *et al.*, "Eigen v3," http://eigen.tuxfamily.org, 2010.

[22] J. Carpentier, F. Valenza, N. Mansard *et al.*, "Pinocchio: fast forward and inverse dynamics for poly-articulated systems," https://stack-of-tasks.github.io/pinocchio, 2015–2021.

[23] J. Pan, S. Chitta, D. Manocha, J. Mirabel, J. Carpentier, and L. Montaut, "Coal - an extension of the Flexible Collision Library," https://github.com/coal-library/coal, 2025.